Surface tension of quark matter in a geometrical approach

Marcus B. Pinto,[1] Volker Koch,[2] and Jørgen Randrup[2]
[1]*Departamento de Física, Universidade Federal de Santa Catarina, 88040-900 Florianópolis, Santa Catarina, Brazil*
[2]*Nuclear Science Division, Lawrence Berkeley National Laboratory, Berkeley, California 94720, USA*
(Received 29 July 2012; published 27 August 2012)

The surface tension of quark matter plays a crucial role for the possibility of quark matter nucleation during the formation of compact stellar objects, because it determines the nucleation rate and the associated critical size. However, this quantity is not well known and the theoretical estimates fall within a wide range, $\gamma_0 \approx$ 5–300 MeV/fm^2. We show here that once the equation of state is available one may use a geometrical approach to obtain a numerical value for the surface tension that is consistent with the model approximations adopted. We illustrate this method within the two-flavor linear σ model and the Nambu–Jona-Lasinio model with two and three flavors. Treating these models in the mean-field approximation, we find $\gamma_0 \approx$ 7–30 MeV/fm^2. Such a relatively small surface tension would favor the formation of quark stars and may thus have significant astrophysical implications. We also investigate how the surface tension decreases towards zero as the temperature is raised from zero to its critical value.

DOI: 10.1103/PhysRevC.86.025203 PACS number(s): 21.65.Qr, 11.10.Wx, 12.39.Ki, 26.60.Kp

I. INTRODUCTION

Lattice-gauge calculations yield a nonvanishing value of the quark condensate $\langle\bar{\psi}\psi\rangle$ in the QCD vacuum [1], indicating that chiral symmetry is broken. This general feature of the vacuum remains present even for massless quarks because the symmetry is then broken spontaneously. However, chiral symmetry is expected to become restored at sufficiently high values of the net-baryon density ρ or/and the temperature T. The character of this phase change is not yet well understood but it has significant implications in areas such as cosmology and astrophysics and it is a focal point for current experimental and theoretical research in nuclear physics.

Nuclear collision experiments carried out with the Relativistic Heavy Ion Collider (RHIC) at the Brookhaven National Laboratory and with the Large Hadron Collider at CERN explore systems having relatively small net-baryon densities ρ and the associated chemical potentials μ are negligible. Lattice calculations can readily be carried out at vanishing μ and they indicate that a cross-over transformation from the chirally broken phase to the restored phase occurs as the temperature is increased from below to above the cross-over temperature $T_\times \approx 160$ MeV [1–3].

The other extreme region of the QCD phase diagram, namely low temperatures and high chemical potentials, cannot be addressed by current lattice-QCD methods, owing to the fermion sign problem, and studies of this phase region must therefore rely on less fundamental models. Most investigations suggest that there is a first-order phase transition which, for $T \approx 0$, sets in at baryon densities several times that of the nuclear saturation density, $\rho_0 \approx 0.153/\text{fm}^3$. The properties of strongly interacting matter in this phase region are important for our understanding of compact stars.

If indeed such a first-order phase transition exists at $T = 0$, then, as the temperature is raised, one would expect it to remain present but gradually weaken and eventually terminate at a critical point (μ_c, T_c). The existence and location of such a critical point is a subject of intense theoretical investigation with a variety of models, including in particular effective-field models, such as the linear σ model (LSM), and effective quark models, such as the Nambu–Jona-Lasinio (NJL), at different levels of sophistication considering up to three quark flavors and possibly including the Polyakov loop to account for confinement [4,5]. Experimentally, the corresponding region of density and excitation may be produced in current nuclear collisions at the low-energy end of RHIC and in the future with FAIR at GSI and NICA at JINR, which are being constructed with such investigations in mind.

In the present work, we concentrate on the high-μ and low-T part of the phase diagram with the aim of exploring the expected chiral phase transition which has significant implications for the possible existence of quark stars [6,7]. It should be noted that chiral symmetry may be restored already during the early postbounce accretion stage of a core-collapse supernova event and the associated neutrino burst might then provide a spectacular signature for the presence of quark matter inside compact stars [8]. However, as pointed out in Refs. [9,10], the possibilities depend on the dynamics of the phase conversion and especially on the time scales involved.

When the phase diagram of bulk matter exhibits a first-order phase transition, the two phases may coexist in mutual thermodynamic equilibrium and, consequently, when brought into physical contact a mechanically stable interface will develop between them. The associated interface tension γ_T (which we shall often refer to simply as the surface tension of quark matter) depends on the temperature T; it has its largest magnitude at $T = 0$ and approaches zero as T is increased to T_c. This quantity plays a key role in the phase conversion process and it is related to various characteristic quantities such as the nucleation rate, the critical bubble radius, and the favored scale of the blobs generated by the spinodal instabilities [11,12]. (As we shall see, the surface tension is essentially proportional to the effective interaction range, which determines the width of the surface region, and the spatial size of the most rapidly amplified density irregularity is also proportional to this quantity.)

Unfortunately, despite its central importance, the surface tension of quark matter is rather poorly known. Estimates in the literature fall within a wide range, typically $\gamma_0 \approx$ 10–50 MeV/fm^2 [13,14] and values of $\gamma_0 \approx 30$ MeV/fm^2 have been considered for studying the effect of quark-matter nucleation on the evolution of protoneutron stars [15]. However, the authors of Ref. [16], taking into account the effects from charge screening and structured mixed phases, estimate $\gamma_0 \approx 50$–150 MeV/fm^2, without excluding smaller values, and an ever higher value, $\gamma_0 \approx 300$ MeV/fm^2, was found by Alford *et al*. [17] on the basis of dimensional analysis of the minimal interface between a color-flavor locked phase and nuclear matter.

The surface tension for two-flavor quark matter was evaluated within the framework of the LSM by Palhares and Fraga [18]. In that work the authors considered the one-loop effective potential and then fitted its relevant part, which included both the chirally symmetric and the broken state, by a quartic polynomial. The surface tension was evaluated using the thin-wall approximation for bubble nucleation and the estimated values cover the 5–15 MeV/fm^2 range, depending on the inclusion of vacuum and/or thermal corrections. In principle, this range makes nucleation of quark matter possible during the early postbounce stage of core-collapse supernovae and it is thus a rather important result. It is also worth noting that a small surface tension would facilitate various structures in compact stars, including mixed phases [19].

The present work is devoted to the evaluation of the surface tension for quark matter using both the LSM (with two flavors) and the NJL model (with two and three flavors) following the procedure employed in Ref. [12]. Here, the LSM is mainly included to check the consistency of our procedure by comparing our present results with those obtained by the thin-wall approximation of Ref. [18] (we find the agreement to be very good). The NJL model is considered with two and three flavors because the latter, which contains strangeness, is one of the most popular effective quark models used in studies related to compact stars. As explained below, the method described in Ref. [12] makes it possible to express the surface tension for any subcritical temperature in terms of the free energy density for uniform matter in the unstable density range. Because the models employed readily provide the equation of state (EoS) for the full density range, they are well suited for our purpose and we may directly employ the method without any further approximations. In practice, the procedure is rather simple to implement and it provides an estimate for the surface tension that is consistent with the EoS implied by the model employed, with its specific approximations and parametrizations.

The paper is organized as follows. In Sec. II we review the method for extracting the surface tension from the EoS. In Sec. III we then present the two-flavor versions of the two models considered and discuss how to extract the surface tension. Section IV is devoted to the treatment for the more realistic SU(3) version of the NJL model and our numerical results are presented in Sec. V, both for cold matter and for temperatures up to the critical value. The conclusions and final remarks are presented in Sec. VI.

II. THE GEOMETRIC APPROACH TO THE SURFACE TENSION EVALUATION

We assume here that the material at hand, strongly interacting matter, may appear in two different phases under the same thermodynamic conditions of temperature T, chemical potential μ, and pressure P. These two coexisting phases have different values of other relevant quantities, such as the energy density $\mathcal{E}$, the (net baryon) density ρ, and the entropy density s. Under such circumstances, the two phases will develop a mechanically stable interface if placed in physical contact and it is the purpose of the present study to evaluate the associated interface tension, γ_T.

The two-phase feature appears for all temperatures below the critical value, T_c. Thus, for any subcritical temperature, $T < T_c$, hadronic matter at the (net-baryon) density $\rho_1(T)$ has the same chemical potential and pressure as quark matter at the (larger) density $\rho_2(T)$. As T is increased from zero to T_c, the coexistence phase points (ρ_1, T) and (ρ_2, T) trace out the lower and higher branches of the phase coexistence boundary, respectively, gradually approaching each other and finally coinciding for $T = T_c$. Any (ρ, T) phase point outside of this boundary corresponds to thermodynamically stable uniform matter, whereas uniform matter prepared with a density and temperature corresponding to a phase point inside the phase coexistence boundary is thermodynamically unstable and prefers to separate into two coexisting thermodynamically stable phases separated by a mechanically stable interface. Because such a two-phase configuration is in global thermodynamic equilibrium, the local values of T, μ, and P remain unchanged as one moves from the interior of one phase through the interface region and into the interior of the partner phase, as the local density ρ increases steadily from the lower coexistence value ρ_1 to the corresponding higher coexistence value ρ_2.

It is convenient to work in the canonical framework in which the control parameters are temperature and density. The basic thermodynamic function is thus $f_T(\rho)$, the free energy density as a function of the (net baryon) density ρ for the specified temperature T. The chemical potential can then be recovered as $\mu_T(\rho) = \partial_\rho f_T(\rho)$, and the entropy density as $s_T(\rho) = -\partial_T f_T(\rho)$, so the energy density is $\mathcal{E}_T(\rho) = f_T(\rho) - T\partial_T f_T(\rho)$, while the pressure is $P_T(\rho) = \rho\partial_\rho f_T(\rho) - f_T(\rho)$.

For single-phase systems $f_T(\rho)$ is convex; that is, its second derivative $\partial_\rho^2 f_T(\rho)$ is positive, while the appearance of a concavity in $f_T(\rho)$ signals the occurrence of phase coexistence, at that temperature. This is easily understood because when $f_T(\rho)$ has a local concave anomaly then there exist a pair of densities, ρ_1 and ρ_2, for which the tangents to $f_T(\rho)$ are common. Therefore, $f_T(\rho)$ has the same slope at those two densities, so the corresponding chemical potentials are equal, $\mu_T(\rho_1) = \partial_\rho f_T(\rho_1) = \partial_\rho f_T(\rho_2) = \mu_T(\rho_2)$. Furthermore, because a linear extrapolation of $f_T(\rho)$ leads from one of the touching points to the other, also the two pressures are equal, $P_T(\rho_1) = \rho_1\partial_\rho f_T(\rho_1) - f_T(\rho_1) = \rho_2\partial_\rho f_T(\rho_2) - f_T(\rho_2) = P_T(\rho_2)$. So uniform matter at the density ρ_1 has the same temperature, chemical potential, and pressure as uniform matter at the density ρ_2. The common tangent between the two coexistence points corresponds to

the familiar Maxwell construction and shall here be denoted as $f_T^M(\rho)$. Obviously, $f_T(\rho)$ and $f_T^M(\rho)$ coincide at the two coexistence densities and, furthermore, $f_T(\rho)$ exceeds $f_T^M(\rho)$ for intermediate densities. Therefore, we have $\Delta f_T(\rho) \equiv f_T(\rho) - f_T^M(\rho) \geqslant 0$.

For a given (subcritical) temperature T, we now consider a configuration in which the two coexisting bulk phases are placed in physical contact along a planar interface. The associated equilibrium profile density is denoted by $\rho_T(z)$, where z denotes the location in the direction normal to the interface. In the diffuse interface region, the corresponding local free energy density, $f_T(z)$, differs from what it would be for the corresponding Maxwell system; that is, a mathematical mix of the two coexisting bulk phases with the mixing ratio adjusted to yield an average density equal to the local value $\rho(z)$. This local deficit amounts to

$$\delta f_T(z) \;=\; f_T(z) - f_i - \frac{f_T(\rho_2) - f_T(\rho_1)}{\rho_2 - \rho_1}\,[\rho_T(z) - \rho_i], \quad (1)$$

where ρ_i is either one of the two coexistence densities. The function $\delta f_T(z)$ is smooth and it tends quickly to zero away from the interface where $\rho_T(z)$ rapidly approaches ρ_i and $f_T(z)$ rapidly approaches $f_T(\rho_i)$. The interface tension γ_T is the total deficit in free energy per unit area of planar interface,

$$\gamma_T \;=\; \int_{-\infty}^{+\infty} \delta f_T(z)\, dz. \quad (2)$$

As discussed in Ref. [12], when a gradient term is used to take account of finite-range effects, the tension associated with the interface between the two phases can be expressed without explicit knowledge about the profile functions but exclusively in terms of the EoS for uniform (albeit unstable) matter,

$$\gamma_T \;=\; a \int_{\rho_1(T)}^{\rho_2(T)} [2\mathcal{E}_g \Delta f_T(\rho)]^{1/2} \frac{d\rho}{\rho_g}, \quad (3)$$

where ρ_g is a characteristic value of the density and $\mathcal{E}_g$ is a characteristic value of the energy density, while the parameter a is an effective interaction range related to the strength of the gradient term, $C = a^2\mathcal{E}_g/\rho_g^2$. We choose the characteristic phase point to be in the middle of the coexistence region, $\rho_g = \rho_c$ and $\mathcal{E}_g = [\mathcal{E}_0(\rho_c) + \mathcal{E}_c]/2$, where $\mathcal{E}_0(\rho_c)$ is energy density at $(\rho_c, T = 0)$, while $\mathcal{E}_c$ is energy density at the critical point (ρ_c, T_c). The length a as a somewhat adjustable parameter governing the width of the interface region and the magnitude of the tension [12]. For the LSM it is natural to expect that $a \approx 1/m_\sigma \approx 0.33$ fm which, also, is approximately the value found in an application of the Thomas-Fermi approximation to the NJL model [20]. Therefore, we shall adopt the value $a = 0.33$ fm throughout the present work. While there is some arbitrariness in fixing these quantities, it is reassuring that the resulting surface tension is in excellent agreement with the value obtained in Ref. [18].

With these parameters fixed, the interface tension can be calculated once the free energy density $f_T(\rho)$ is known for uniform matter in the unstable phase region, $\rho_1(T) \leqslant \rho \leqslant \rho_2(T)$. While this is straightforward in a canonical formulation, where each (ρ, T) characterizes only one manifestation of the system, even inside the unstable phase region, the task is more complicated in the commonly used grand canonical formulation because a given (μ, T) phase point characterizes three different manifestations of the system, one stable, one metastable, and one unstable. The metastable solutions are located near the coexistence densities, while the unstable solutions are located in the intermediate spinodal region where uniform matter is mechanically unstable so that even infinitesimal irregularities may be exponentially amplified. By contrast, only irregularities of a sufficient amplitude are amplified in the metastable regions, leading towards either nucleation (near the lower coexistence density ρ_1) or bubble formation (near the higher coexistence density ρ_2).

III. THE EOS FOR THE EFFECTIVE TWO-FLAVOR QUARK MODELS

In this section, we review the mean-field results for the thermodynamic potential for the two effective models when only two quark flavors are included. These results have been widely discussed in the literature and here we follow Ref. [21] (see Ref. [22] for results beyond the mean-field approximation). The two models are similar in the sense that they do not have confinement and they incorporate spontaneous chiral symmetry breaking, which happens at the classical level in the LSM but only via quantum corrections in the NJL model. The fermionic fields representing the quarks are the only degrees of freedom in the NJL model at the tree level, while the LSM also contains scalar (σ) and pseudoscalar ($\boldsymbol{\pi}$) meson fields.

A. The linear σ model

In standard notation, the Lagrangian density of the LSM with quarks reads

$$\begin{aligned}\mathcal{L}_{\rm LSM} \;&=\; \tfrac{1}{2}(\partial_\mu \boldsymbol{\pi})^2 + \tfrac{1}{2}(\partial_\mu \sigma)^2 - U(\sigma, \boldsymbol{\pi}) \\ &\quad + \bar{\psi}[\mathrm{i}\gamma^\mu \partial_\mu - g(\sigma + \mathrm{i}\gamma_5 \boldsymbol{\tau}\cdot\boldsymbol{\pi})]\psi, \end{aligned} \quad (4)$$

where ψ is the flavor isodoublet spinor representing the quarks (u and d), and

$$U(\sigma, \boldsymbol{\pi}) \;=\; \frac{\lambda^2}{4}(\sigma^2 + \boldsymbol{\pi}^2 - v^2)^2 - H\sigma \quad (5)$$

is the classical potential energy density. In the chiral limit (obtained for $H = 0$) the chiral symmetry, $\mathrm{SU}(2)_V \times \mathrm{SU}(2)_A$, is spontaneously broken at the classical level, and the pion is the associated massless Goldstone boson. For $H \neq 0$, the chiral symmetry is explicitly broken by the last term in $U(\sigma, \boldsymbol{\pi})$, which gives the pion a finite mass at vanishing T and μ. The parameters are usually chosen so that chiral symmetry is spontaneously broken in the vacuum and the expectation values of the meson fields are $\langle\sigma\rangle = f_\pi$ and $\langle\boldsymbol{\pi}\rangle = \mathbf{0}$, where $f_\pi = 93$ MeV is the pion decay constant. Following Ref. [21], we fix the parameters as follows: $v^2 \simeq (87.73\ \mathrm{MeV})^2$, $\lambda^2 \simeq 20$, and $H \simeq (12.1\ \mathrm{GeV})^3$. Using the standard relations, $H = f_\pi m_\pi^2$, $v^2 = f_\pi^2 - m_\pi^2/\lambda^2$, and $m_\sigma^2 = 2\lambda^2 f_\pi^2$, we obtain the meson masses, $m_\pi = 138$ MeV and $m_\sigma = 600$ MeV. The coupling constant g is usually fixed

so that the effective quark mass in vacuum, $M^{\rm vac} = gf_\pi$, is about one-third of the nucleon mass, which gives $g \simeq 3.3$. We note that the same parameter set was also used to evaluate the surface tension, γ_T, in Ref. [18]. To the one-loop level, the grand canonical potential is obtained by integrating the action over the fermionic fields [21],

$$\begin{aligned}&\Omega_{\rm LSM}(\sigma, \boldsymbol{\pi}; T, \mu_q)\\ &\quad = U(\sigma, \boldsymbol{\pi}) - 2N_f N_c \int \frac{d^3\boldsymbol{p}}{(2\pi)^3}\{E - T\ln[1-n^+]\\ &\qquad - T\ln[1-n^-]\},\end{aligned} \tag{6}$$

where $N_c = 3$, $N_f = 2$, $E^2 = \boldsymbol{p}^2 + M^2$, and $n^\pm = \{1 + \exp[(E \mp \mu_q)/T]\}^{-1}$ represent the particle/antiparticle thermal occupancies with $\mu_q = \mu_u = \mu_d$, where $\mu = 3\mu_q$. For given values of T and μ, the equilibrium values of the meson fields are obtained by minimizing $\Omega(\sigma, \boldsymbol{\pi}; T, \mu_q)$ with respect to those, yielding the most likely values $\underline{\sigma}$ and $\underline{\boldsymbol{\pi}}$. The latter one vanishes in the mean-field approximation, so the associated constituent quark mass is given as $M^2 = g^2\underline{\sigma}^2$. The minimum value of the grand potential represents minus the equilibrium pressure, $\Omega_{\rm min}(T, \mu) = -P$, so the net quark density is given by $\rho_q = (\partial P/\partial\mu_q)_T$, where $\rho_q = 3\rho$. The entropy density given by $s = (\partial P/\partial T)_{\mu_q}$, while the energy density, $\mathcal{E}$, can then be obtained by means of the standard thermodynamic relation $P = Ts - \mathcal{E} + \mu\rho$ and the free energy density is $f \equiv \mathcal{E} - Ts = \mu\rho - P$.

In the neighborhood of the phase coexistence line in the (μ, T) plane, the grand potential has three extrema representing stable, metastable, and spinodally unstable matter. As emphasized above, the extraction of the surface tension by the geometric approach requires the consideration of all three extrema.

In contrast to the NJL model, the vacuum term represented by the first term in the integrand of Eq. (6) is not essential for the spontaneous breaking of chiral symmetry. In the LSM this already happens at the classical level and the symmetry restoration is driven mainly by the terms containing $n^\pm$. Therefore, we neglect the vacuum term in the present LSM application, where the aim is to compare our estimates with the zero-temperature interface tension obtained in Ref. [18], $\gamma_0 \simeq 12.98$ MeV/fm^2, where the relevant part of the same thermodynamical potential was fitted with a quartic polynomial. In our approach such a fitting procedure is not necessary because the thermodynamic potential is evaluated for all values of μ and T. This will lead to somewhat different numerical values for the surface tension γ_T. It was shown in Ref. [18] that the inclusion of vacuum terms at $T = 0$ increases the surface tension value from $\gamma_0 = 12.98$ MeV/fm^2 to about $\gamma_0 \simeq 17$ MeV/fm^2. In practice, further refinements including vacuum and in-medium two-loop corrections are possible by following the same technical steps that were employed in the evaluation of the thermodynamical potential for the Yukawa theory [23].

It is now straightforward to determine the phase-coexistence line in the (μ, T) plane which forms the starting point for determining all quantities related to γ_T. It starts at $(\mu = 918$ MeV, $T = 0)$ and terminates at the critical point $(\mu_c = 621$ MeV, $T_c = 99$ MeV), which agrees with Ref. [21].

We now have all the ingredients needed for determining the coexistence densities $\rho_1(T)$ and $\rho_2(T)$ as well as the characteristic values ρ_g and $\mathcal{E}_g$ appearing in Eq. (3).

The difference $\Delta f(\rho)$ can be readily determined numerically by considering the stable (global) minimum, the metastable (local) minimum, and the unstable (local) maximum appearing in the thermodynamical potential, as will be explicitly shown in Sec. V. Although our method for extracting the surface tension does not require the profiles $\sigma(z)$ and $\rho(z)$, these functions do provide interesting additional information about the interface. To obtain the profile functions within the LSM, it suffices to consider the grand canonical potential in the σ direction only, that is, taking $\boldsymbol{\pi} = \boldsymbol{0}$. At $T = 0$ it can be expressed in terms of the Fermi momentum p_F (given by $p_F^2 = \mu_q^2 - g^2\sigma^2$),

$$\begin{aligned}&\Omega_{\rm LSM}(\sigma, \boldsymbol{\pi} = \boldsymbol{0}; T = 0, \mu)\\ &\quad = U(\sigma) - \frac{N_f N_c}{24\pi^2}\left\{2\mu_q p_F^3 - 3(g\sigma)^2\left[\mu_q p_F\right.\right.\\ &\qquad \left.\left. - (g\sigma)^2 \ln\left(\frac{p_F + \mu_q}{g\sigma}\right)\right]\right\}.\end{aligned} \tag{7}$$

We now employ the local density approximation, so the local Fermi momentum, $p_F(\boldsymbol{r})$, is related to the local density, $\rho_q(\boldsymbol{r}) \equiv \langle\psi^+\psi\rangle$, by $\rho_q = (N_c N_f/3\pi^2)p_F^3(\boldsymbol{r})$. Furthermore, the local scalar density $\rho_s(\boldsymbol{r}) \equiv \langle\overline{\psi}\psi\rangle$ is given by

$$\begin{aligned}&\rho_s(\boldsymbol{r})\\ &\quad = 2N_c N_f \int \frac{d^3p}{(2\pi)^3}\frac{M(\boldsymbol{r})}{\sqrt{p^2 + M(\boldsymbol{r})^2}}\\ &\quad = \frac{N_c N_f}{2\pi^2} g\sigma(\boldsymbol{r})\left[\mu_q p_F(\boldsymbol{r}) - g^2\sigma(\boldsymbol{r})^2 \ln\left(\frac{p_F(\boldsymbol{r}) + \mu_q}{g\sigma(\boldsymbol{r})}\right)\right],\end{aligned} \tag{8}$$

where we have used that the local Fermi energy $E_F(\boldsymbol{r}) = \sqrt{p_F(\boldsymbol{r})^2 + M(\boldsymbol{r})^2}$ equals the (constant) chemical potential $\mu_q = \mu/3$. We note that

$$[\partial_\sigma \Omega_{\rm LSM}(\sigma, \boldsymbol{0}; 0, \mu)]_{\sigma=\sigma(\boldsymbol{r})} = U'(\sigma(\boldsymbol{r})) + g\rho_s(\boldsymbol{r}). \tag{9}$$

Then the stationary Euler-Lagrange equation with $\boldsymbol{\pi} = \boldsymbol{0}$ and $\overline{\psi}\psi$ replaced with $\rho_s(\boldsymbol{r})$ provides an equation for the local value of the order parameter, $\sigma(\boldsymbol{r})$,

$$\boldsymbol{\nabla}^2\sigma(\boldsymbol{r}) - [U'(\sigma(\boldsymbol{r})) + g\rho_s(\boldsymbol{r})] = 0. \tag{10}$$

For semi-infinite geometry, the profile of the order parameter, $\sigma(z)$, can then be obtained by solving the corresponding Euler-Lagrange equation,

$$\partial_z^2\sigma(z) - [\partial_\sigma \Omega_{\rm LSM}(\sigma)]_{\sigma=\sigma(z)} = 0, \tag{11}$$

with the boundary conditions that the order parameter approach the zero-temperature coexistence values far from the surface,

$$\begin{aligned}&\sigma(z \to -\infty) \to \sigma_1(T = 0) = f_\pi,\\ &\sigma(z \to +\infty) \to \sigma_2(T = 0) = 0.13\, f_\pi.\end{aligned} \tag{12}$$

Once $\sigma(z)$ is known, so is the mass $M(z)$, and we can then obtain the local Fermi momentum $p_F(z)$ and, consequently,

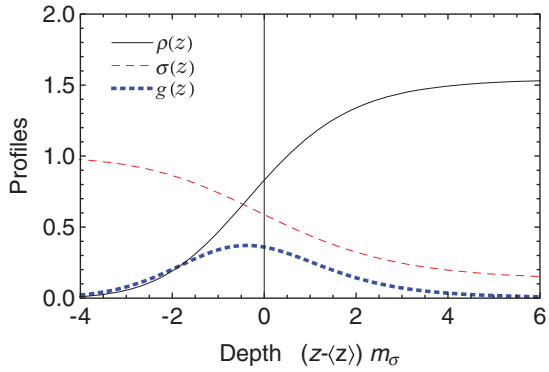

FIG. 1. (Color online) The order parameter $\sigma(z)$ in units of f_π (dashed curve), the net baryon density $\rho(z)$ in units of ρ_0 (solid curve), and the surface location function $g(z)$ (dotted curve), as functions of the dimensionless depth $(z - \langle z\rangle)m_\sigma$ relative to the average surface location.

the local net baryon density $\rho(z)$. One may then define the associated interface location function [12,24],

$$g(z) \equiv \frac{\partial_z \rho(z)}{\rho_2 - \rho_1}, \tag{13}$$

which allows us to obtain additional information, such as the mean interface location, $\bar{z} = \langle z\rangle \equiv \int z g(z) dz$, the associated interface width, b, where $b^2 = \langle (z - \bar{z})^2\rangle$, as well as a measure of the profile skewness, which is given by the dimensionless parameter $\gamma_3 \equiv \langle (z - \bar{z})^3\rangle / b^3$ [24]. The calculated results for $\sigma(z)$, $\rho(z)$, and $g(z)$ are shown in Fig. 1. The origin is conveniently located at $\langle z\rangle$, the width is $b = 1.85\,a$ (where $a = 1/m_\sigma \approx 0.33$ fm), and the skewness is $\gamma_3 = 0.6$. As the temperature is increased, the profiles widen progressively and grow more symmetric, also found in Ref. [12].

B. The Nambu–Jona-Lasino model

We now consider the standard version of the two-flavor NJL model [25]. Its Lagrangian density is based on a chirally symmetric four-fermion interaction,

$$\mathcal{L}_{\rm NJL} = \bar{\psi}(i\gamma_\mu \partial^\mu - m)\psi + G[(\bar{\psi}\psi)^2 + (\bar{\psi} i\gamma_5 \vec{\tau}\psi)^2], \tag{14}$$

where ψ is to be interpreted as in the LSM. Furthermore, it is assumed that $m_u = m_d$ so the mass matrix is given by $m_c = m\,\mathrm{diag}(1, 1)$. In the mean-field approximation, the grand canonical potential reads [21,22,26]

$$\Omega_{\rm NJL}(\mu, T) = \frac{(M - m)^2}{4G} - 2N_f N_c \int_{p<\Lambda} \frac{d^3\boldsymbol{p}}{(2\pi)^3} \times \{E - T\ln[1 - n^+] - T\ln[1 - n^-]\}, \tag{15}$$

with the same definitions as used in the LSM. For each value of T and μ the dynamical mass is of the form $M\,\mathrm{diag}(1, 1)$ because of the assumption of isospin symmetry ($m_u = m_d = m$) and chemical equilibrium ($\mu_u = \mu_d = \mu$); alternative scenarios may also be considered [27]. The single dynamical mass M is then obtained by minimizing Ω with respect to M, leading to the well-known gap equation,

$$M = m + 2GN_c N_f \int_{p<\Lambda} \frac{d^3\boldsymbol{p}}{(2\pi)^3} \frac{M}{E}[1 - n^+ - n^-]. \tag{16}$$

Although the thermodynamic potentials for LSM [Eq. (6)] and the NJL model [Eq. (15)] have the same structure as far as the loop contribution is concerned, some important differences between the two models exist. First, we note that within the NJL the quark mass acquires its constituent value only when quantum corrections (loop terms) are computed. Therefore, contrary to the LSM, the divergent term represented by the second term on the right-hand side of Eq. (15) plays a central role regarding the (dynamical) chiral symmetry breaking. Another difference between the LSM and the NJL model, in $3 + 1$ dimensions, is that the latter is not renormalizable because the coupling G carries dimensions (energy^{-2}). This means that potential divergencies cannot be systematically eliminated by a redefinition of the original parameters. By considering it as an effective model, one gives up the very high energies and evaluates all the integrals up to an ultraviolet (noncovariant) cutoff Λ, as the notation in Eqs. (15) and (16) implies. Then Λ is treated as a "parameter" which will be fixed, together with G and m, so as to yield the values of physical observables such as m_π, f_π that reproduce the phenomenological value of $\langle\bar{\psi}\psi\rangle$. For example, in Ref. [21] the authors reproduce $f_\pi = 93$ MeV and $m_\pi = 138$ MeV using $\Lambda = 631$ MeV and $G\Lambda^2 = 2.19$ with $m = 5.5$ MeV. These parameter values, which we label "set I," predict a first-order phase transition starting at $T = 0$, $\mu = 1045.5$ MeV and ending at the critical point ($T_c = 46$ MeV, $\mu_c = 996$ MeV), while the constituent quark mass in vacuum is $M^{\rm vac} = 337$ MeV. In their study of the chiral phase transition in the presence of spinodal decomposition the authors of Ref. [26] use $\Lambda = 587.9$ MeV and $G\Lambda^2 = 2.44$ with $m = 5.6$ MeV to reproduce $f_\pi = 92.4$ MeV and $m_\pi = 135$ MeV, obtaining $M^{\rm vac} = 400$ MeV. We also consider these parameter values, which we label "set II," to estimate the influence of different parametrizations in the estimation of γ_T. With parameter set II the first-order transition line starts at ($T = 0$, $\mu = 1146.3$ MeV) and ends at ($T_c = 81$ MeV, $\mu_c = 990$ MeV). In general, a larger value of $G\Lambda^2$ enlarges the coexistence region. As in the LSM case, the quantities ρ_1, ρ_2, ρ_g, $\mathcal{E}_g$, and $\Delta f(\rho)$ entering the expression (3) for the surface tension can be obtained from the EoS. As already emphasized, the numerical value for the length scale a is chosen to be $1/m_\sigma \simeq 0.33$ fm (which is about the value found in a Thomas-Fermi application to the NJL model [20]). The remaining two numerical inputs, ρ_g and ϵ_g, are automatically fixed once the EoS has been determined.

IV. THE EOS FOR THE NJL MODEL WITH THREE QUARK FLAVORS

In stellar modeling, the structure of the star depends on the assumed EoS built with appropriate models while the true ground state of matter remains a source of speculation. It has been argued [28–31] that *strange quark matter* (SQM) is the true ground state of all matter and this hypothesis is

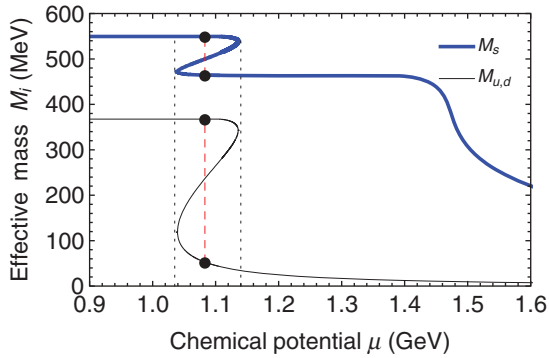

FIG. 2. (Color online) The constituent quark masses as functions of the baryon chemical potential μ for $T = 0$ in the three-flavor NJL model. The top curve shows M_s, while the bottom curve represents $M_u = M_d$. Phase coexistence occurs at $\mu = 1083$ MeV and the corresponding mass values are indicated by the dots. These are are joined by the Maxwell curves (dashed) that trace out the gradual phase conversion when full equilibrium is maintained; M_s then decreases from 549 to 464.4 MeV, while $M_u = M_d$ decreases from 367.6 to 52.5 MeV. Between the two dotted curves there are three solutions for a given μ: stable matter, metastable matter, and (between the two extrema) spinodally unstable matter.

known as the Bodmer-Witten conjecture. Hence, the interior of neutron stars should be composed predominantly of u, d, s quarks (plus leptons if one wants to ensure charge neutrality which is not the case in the present work). Strangeness is implemented in the SU(3) version of the NJL model, which is given by

$$\begin{aligned}\mathcal{L} &= \bar{\psi}(i\gamma_\mu\partial^\mu - m)\psi + G\sum_{a=0}^{8}[(\bar{\psi}\lambda^a\psi)^2 + (\bar{\psi}i\gamma_5\lambda^a\psi)^2] \\ &\quad - K\{\det{}_f[\bar{\psi}(1+\gamma_5)\psi] + \det{}_f[\bar{\psi}(1-\gamma_5)\psi]\}, \end{aligned} \tag{17}$$

where $\psi = (u, d, s)^T$ denotes a quark field with three flavors (and three colors) and $m = \mathrm{diag}_f(m_u, m_d, m_s)$ is the corresponding mass matrix. Here we assume $m_u = m_d \neq m_s$, indicating that isospin symmetry is observed while the SU(3) flavor symmetry is explicitly broken. The eight Gell-Mann matrices are represented by λ^a $(a = 1, \ldots, 8)$ and $\lambda^0 = \sqrt{2/3}\,\boldsymbol{I}$. More details concerning this version of the NJL model can be found in Ref. [27]. In the mean-field approximation the thermodynamical potential is given by

$$\Omega_{\mathrm{NJL}_3}(T, \mu_q) = \sum_{q=u,d,s}\left[\Omega_{M_q}(T, \mu_q) + 2G\phi_q^2\right] - 4K\phi_u\phi_d\phi_s. \tag{18}$$

The term Ω_{M_q}, which represents the contribution of a gas of quasiparticles with mass M_q, is given by

$$\begin{aligned}\Omega_{M_q} &= -2N_c\int_{p<\Lambda}\frac{d^3\boldsymbol{p}}{(2\pi)^3}\{E_q - T\ln[1-n_q^+] \\ &\quad - T\ln[1-n_q^-]\}, \end{aligned} \tag{19}$$

where $E_q^2 = \boldsymbol{p}^2 + M_q^2$ and $n_q^\pm = \{1 + \exp[(E_q \mp \mu_q)/T]\}^{-1}$ represent the particle/antiparticle distribution function. For the quark condensates, $\phi_q = \langle\bar{\psi}_q\psi_q\rangle$, one has

$$\phi_q = -2N_c\int_{p<\Lambda}\frac{d^3\boldsymbol{p}}{(2\pi)^3}\frac{M_q}{E_q}[1 - n_q^+ - n_q^-]. \tag{20}$$

Finally, the gap equation is

$$\begin{aligned} M_i &= m_i - 4G\phi_i + 2K\phi_j\phi_k, \\ (i, j, k) &= \text{any permutation of } (u, d, s), \end{aligned} \tag{21}$$

which contains a nonflavor mixing term proportional to G as well as a flavor mixing term proportional to K. In our numerical analysis we adopt the parameter values of Ref. [32] which are $m_u = m_d = 5.5$ MeV, $m_s = 140.7$ MeV, $G\Lambda^2 = 1.835$, $K\Lambda^5 = 12.36$, and $\Lambda = 602.3$ MeV. Then, at $T = 0$ and $\mu_f = 0$, one reproduces $f_\pi = 92.4$ MeV, $m_\pi = 135$ MeV, $m_K = 497.7$ MeV, and $m_{\eta'} = 960.8$ MeV. For the quark condensates one obtains $\phi_u = \phi_d = -(241.9\ \mathrm{MeV})^3$ and $\phi_s = -(257.7\ \mathrm{MeV})^3$. The constituent quark masses are then given by $M_u = M_d = 367.7$ MeV and $M_s = 549.5$ MeV. The pressure, P, and energy density, $\mathcal{E}$, follow from the usual expressions,

$$P = -\Omega_{\mathrm{NJL}_3}(T, \{\mu_q\}) \quad \text{and} \quad P = Ts - \mathcal{E} + \sum_{q=u,d,s}\mu_q\rho_q. \tag{22}$$

Here, for simplicity, we take the chemical equilibrium condition, $\mu_u = \mu_d = \mu_s = \mu_q = \mu/3$, which yields $M_u = M_d$ also at finite T and/or μ. Of course, for a realistic

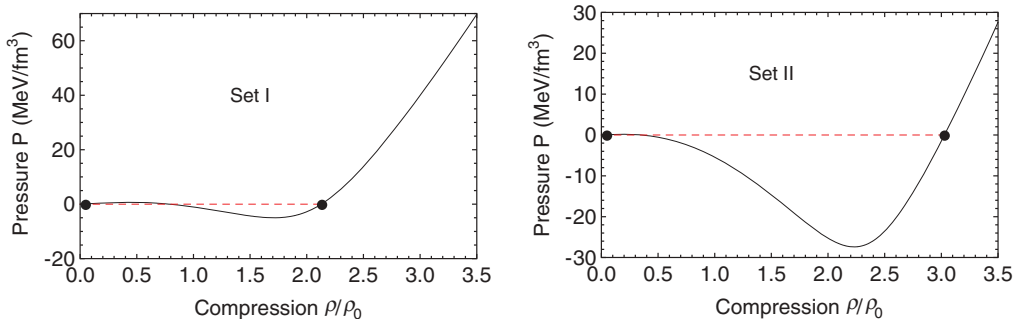

FIG. 3. (Color online) Pressure, P, as a function of compression ρ/ρ_0 for the NJL model as obtained with the two parameter sets. The two coexistence points (dots) are joined by the Maxwell curve (dashed) along which the global equilibrium evolves as the density is increased through the phase coexistence region.

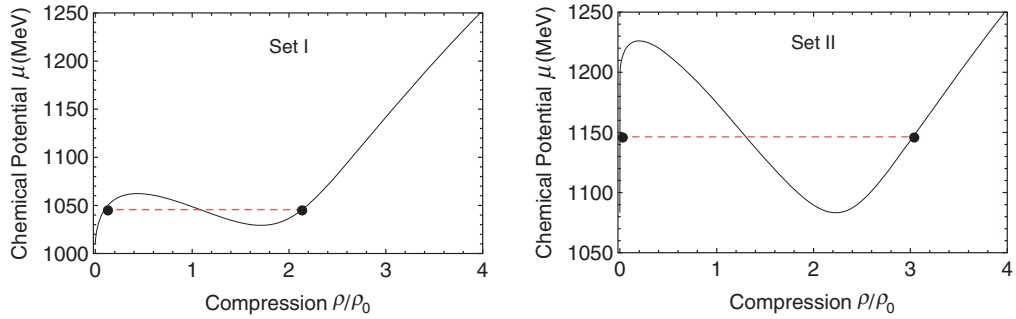

FIG. 4. (Color online) Baryon chemical potential, μ, as a function of compression ρ/ρ_0 for the NJL model as obtained with the two parameter sets. The two coexistence points (dots) are joined by the Maxwell curve (dashed) along which the global equilibrium evolves through the phase coexistence region.

description of neutron-star matter, charge and strangeness neutrality need to be taken into account, which is technically straightforward.

The phase diagram for this three-flavor quark model in the μ-T and ρ-T planes can be found in Ref. [33]; the first-order transition line starts at ($T = 0, \mu = 1083$ MeV) and ends at the critical point ($T_c = 67.7$ MeV, $\mu_c = 955.2$ MeV). As already discussed, we need the EoS inside the phase coexistence region which can be obtained by examining how the effective masses behave in this domain. This behavior is shown in Fig. 2 for $T = 0$; these results go beyond those of Ref. [26] by also considering the strange quark mass. To understand this figure, let us recall that, in most situations, one is generally interested only in those solutions of the gap equation that correspond to global (stable) minima of the thermodynamical potential. However, when a first-order phase transition is present, there are two different such solutions for the same thermodynamic conditions of temperature, chemical potential, and pressure (corresponding to the solid dots on Fig. 2). As the net baryon density (which serves as a convenient order parameter) is increased from its lower coexistence value ρ_1 to its higher coexistence value ρ_2, the thermodynamically favored state is a Maxwell mixture of the two coexisting phases and the overall average of the energy per net baryon or the effective mass, for example, evolve monotonically along the so-called Maxwell line, as the composition of the mixture changes from being entirely one phase to being entirely the other. In the region between the dotted lines the gap equation has three solutions, leading to the back-bending evolution brought in that diagram. It is precisely this typical first-order behavior that will be reflected in the thermodynamical quantities, such as the pressure and densities, as Figs. 3 and 4 show. This behavior is responsible for the fact that there is a (positive) deviation $\Delta f(\rho)$, which then in turn leads to the surface tension.

V. NUMERICAL RESULTS

We now turn to our numerical results for the surface tension γ_T. To this end we need to determine the free energy density $f_T(\rho)$, which requires the evaluation of $P_T(\rho)$ and $\mu_T(\rho)$ for uniform matter thermodynamically unstable region of the phase diagram. For the considered temperature T, the associated density region is bounded by the two coexistence densities ρ_1 and ρ_2, for which the chemical potential μ has the same value, as does the pressure P. As the density ρ is increased through the lower mechanically metastable (nucleation) region, μ and P rise steadily until the lower spinodal boundary has been reached. Then, as ρ moves through the mechanically unstable (spinodal) region, both μ and P decrease until the higher spinodal boundary is reached. They then increase again as ρ moves through the higher mechanically metastable (bubble-formation) region, until they finally regain their original values at $\rho = \rho_2$. It is convenient to express the (net) baryonic density ρ in units of the nuclear

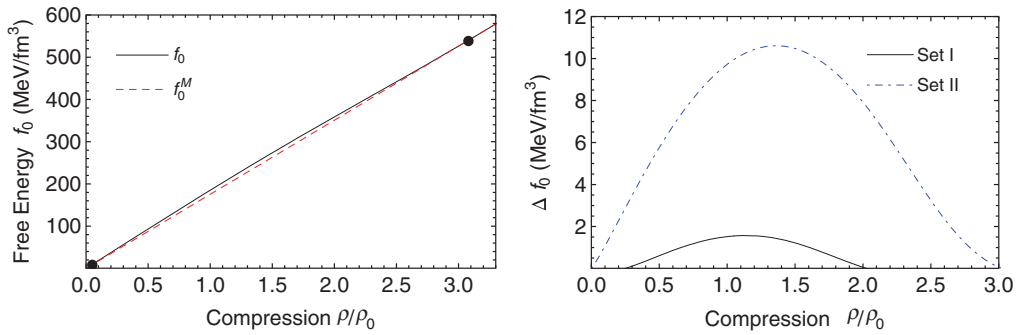

FIG. 5. (Color online) (Left) Free energy density at zero temperature $f_0(\rho)$ (solid curve) and the associated Maxwell curve $f_0^M(\rho)$ (dashed curve) as functions of compression ρ/ρ_0 for the NJL model with parameter set II. The Maxwell curve is tangent to $f_0(\rho)$ at the two coexistence densities $\rho_1 = 0$ and $\rho_2 = 3.027\,\rho_0$. (Right) Quantity $\Delta f_0(\rho)$ as a function of ρ/ρ_0 obtained with the NJL model for parameter set I (solid curve) and parameter set II (dot-dashed curve).

TABLE I. Summary of inputs and results. The length parameter was taken as $a = 0.33$ fm. The zero-temperature bag constant $\mathcal{B}_0$ and the characteristic energy density $\mathcal{E}_g$ are given in MeV/fm^3, while the effective quark masses in vacuum $M_i^{\rm vac}$ as well as the critical values μ_c and T_c are in MeV. The resulting zero-temperature surface tension γ_0 (given in MeV/fm^2) may be compared with the value $\gamma_0 = 12.98$ MeV/fm^2 obtained in Ref. [18]) with the LSM in the thin-wall approximation.

Model	γ_0	$\mathcal{B}_0$	$M_{u,d}^{\rm vac}$	$M_s^{\rm vac}$	T_c	μ_c	ρ_g/ρ_0	$\mathcal{E}_g$
NJL (I)	7.11	100	337	–	46	996	2.00	342.85
NJL (II)	30.25	141.4	400	–	81	990	2.42	495
LSM	13.18	60	306.9	–	99	621	1.19	219.25
NJL$_3$	20.42	291.7	367.6	549.5	67.7	955.2	1.87	326.8

saturation density, $\rho_0 = 0.153/\text{fm}^3$. Generally, as is common practice, we subtract from the pressure any finite value it may have in the vacuum.

A. Zero temperature

Let us start with $T = 0$ for which the relevant results can be readily obtained by taking the $T \to 0$ limit in Eqs. (6) and (15) (see, e.g., Refs. [18,22,27]). Figure 3 shows the pressure as a function of the degree of compression ρ/ρ_0 obtained with the NJL model for both parameter sets I and II; the latter has a stronger coupling and a larger coexistence region. A qualitatively similar behavior is observed in Fig. 4, which shows μ as a function of ρ/ρ_0 for the NJL model with both parameter sets. Figure 5 shows the behavior of the free energy $f_0(\rho)$ and its corresponding Maxwell line $f_0^M(\rho)$ for parameter set II. In the right panel of Fig. 5 we display the difference between these two free energies, $\Delta f(\rho) \equiv f_0(\rho) - f_0^M(\rho)$ for both parameter sets; this is the key quantity for the determination of the surface tension. The LSM and the three-flavor NJL model yield similar results. At temperatures below criticality, $T < T_c$, the thermodynamical potential has two degenerate minima determining the densities of the two coexisting phases, ρ_1 and ρ_2. In all cases studied here, the lower coexistence density vanishes, $\rho_1 = 0$. As for the higher coexistence density, the LSM yields $\rho_2/\rho_0 \simeq 1.54$, the two-flavor NJL model yields $\rho_2/\rho_0 \simeq 2.13$ with set I and $\rho_2/\rho_0 \simeq 3.03$ with set II, while the three-flavor NJL model gives $\rho_2/\rho_0 \simeq 2.62$. It clear from this figure that set I produces a much weaker phase transition because $\Delta f(\rho)$ is much smaller than for set II, as is indeed reflected in the γ_T values shown in Table I. In fact, set II produces a greater coexistence region ($\rho_1 \simeq 0$, $\rho_2 \simeq 3.03\rho_0$, $T_c = 81$ MeV) when compared to set I ($\rho_1 \simeq 0$, $\rho_2 \simeq 2.13\rho_0$, $T_c = 46$ MeV), which is in accordance with the well-known fact that set II should cause the size of the first-order transition line to be longer than the one produced by set I, which has a weaker coupling. Further refinements, such as finite-N_c corrections [34], contributions from thermal fluctuations, and the inclusion of a repulsive vector interaction [35], also tend to shrink the first-order transition line [22] so that, within a fixed parameter set, one should expect these effects to reduce γ_T.

Table I summarizes all our results for γ_0 and also lists the characteristic values $\mathcal{E}_g$ and ρ_g as well as the location of the critical point (T_c, μ_c). The table also provides information related to thermodynamic potential at $T = 0$ and $\mu = 0$ by showing the values of the constituent quark mass in vacuum ($M^{\rm vac}$), which is related to the distance from the global minimum to the origin, as well as the bag constant which gives the energy difference between the local maximum and the global minimum of the potential in vacuum; these values were taken from Refs. [21,27].

We finally note that Palhares and Fraga [18], using the approximation $\gamma_T \approx \int |\partial_z \sigma(z)|^2 dz$ obtained the estimate $\gamma_0 \approx 12.98$ MeV/fm^2, which is very close to our LSM value of 13.18 MeV/fm^2 and also rather similar to the value 12.19 MeV/fm^2 resulting from evaluating that integral using our LSM profile function $\sigma(z)$.

B. Finite temperature

One can easily consider finite temperatures within the employed models. The interface tension is expected to decrease with increasing temperature because both the coexistence densities ρ_i and the associated free energy densities $f_T(\rho_i)$ move closer together at higher T; they ultimately coincide at T_c, where, therefore, the tension vanishes. This general behavior is confirmed by our calculations, as shown in Fig. 6. The LSM, the NJL with parameter set I, and the three-flavor NJL display similar behaviors. The temperature dependence of the surface tension may be relevant for the thermal formation of quark droplets in cold hadronic matter found in "hot" protoneutron stars whose temperatures, T_*, are of the order 10–20 MeV [9,36,37]. For T_* the relevant value of γ_{T_*} may be estimated by using Table I together with Fig. 5. For example, the three-flavor NJL model yields $\gamma_{T_*} \approx 14$–18 MeV/fm^2. The temperature dependence of the surface tension is also

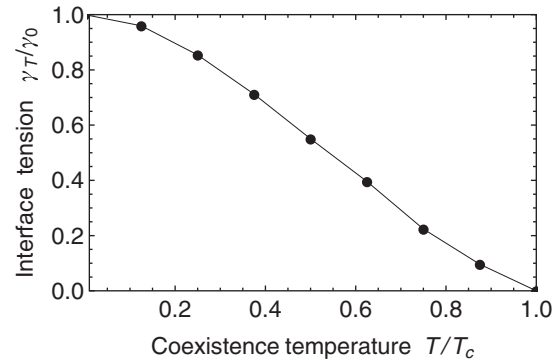

FIG. 6. Surface tension γ_T (relative to its zero-temperature value γ_0) as a function of temperature T (measured relative its critical value T_c), as obtained with the NJL model for parameter set II.

important in the context of heavy-ion collisions, because it determines the favored size of the clumping caused by the action of spinodal instabilities as the expanding matter traverses the unstable phase-coexistence region.

VI. CONCLUSIONS

In this work we have shown that the interface tension related to a first-order phase transition may be evaluated once the uniform-matter EoS is available for the unstable regions of the phase diagram. It is a convenient feature of the method employed that knowledge of the interface profile functions is is not required, because their determination can be quite complicated, as is the case for NJL model [20] (although it is easy for the LSM). In addition to the EoS, the geometrical approach also requires a proper setting of three input parameters, namely the characteristic densities ρ_g and $\mathcal{E}_g$ together with the length scale a. While this does encumber the numerical results with some degree of uncertainty, our zero-temperature LSM result, $\gamma_0 = 13.18\ \mathrm{MeV/fm^2}$, agrees within a few percent with the approximate value obtained in Ref. [18], thus suggesting that those parameters were chosen reasonably.

The surface tension determined in the present fashion is entirely consistent with the employed model, including the approximations and parametrizations adopted. For the effective quark models employed here, this amounts to considering *all* the solutions to the gap equation (stable, metastable, and unstable) and determine the relevant effective quark masses. In most nonperturbative approximations (large N_c, mean field, etc.) the various quantities of interest, such as the free energy density, become functions of this effective mass and will therefore also reflect the metastable and unstable character of the configuration considered. As a cross-check on our procedure, we have evaluated γ_0 for the LSM obtaining a result that differs by only about 2% from estimates based on the thin-wall approximation [18]. We have investigated the two-flavor NJL model as well as its more realistic three-flavor version.

Our main conclusion is that all these effective models generate relatively low values for the the surface tension. This would favor the formation of quark matter and may thus have important astrophysical consequences regarding the existence of pure quark stars. Of particular interest is the three-flavor NJL result, $\gamma_0 = 20.34\ \mathrm{MeV/fm^2}$, because this model is widely used in studies related to neutron stars. Here, for simplicity, we have considered pure quark matter where all flavors share the same chemical potential, but it is just a technical matter to generalize our procedure so as to include leptons (e, μ) to enforce β equilibrium ($\mu_d = \mu_s = \mu_u + \mu_e$, $\mu_e = \mu_\mu$), although the additional chemical potential introduces an increased degree of complexity into the features of the phase transition.

In principle, more refined treatments, such as the Polyakov-NJL model, can also be considered within the same framework. However, because the effects of the Polyakov loop become more important above 100 MeV [38] we believe that our results, especially the three-flavor ones, can be considered as reasonably accurate, although numerical variations may arise owing to the parametrizations and approximations adopted.

ACKNOWLEDGMENTS

M.B.P. was partially supported by CNPq-Brazil, while V.K. and J.R. were supported by the Office of Nuclear Physics in the US Department of Energy's Office of Science under Contract No. DE-AC02-05CH11231. We thank Eduardo Fraga, Sidney Avancini, and Débora Menezes for their comments and suggestions. V.K. would like to thank the Departamento de Física, Universidade Federal de Santa Catarina, for the kind hospitality during the completion of this work.

[1] Y. Aoki, G. Endrodi, Z. Fodor, S. D. Katz, and K. K. Szabo, Nature (London) **443**, 675 (2006).
[2] Y. Aoki, Z. Fodor, S. D. Katz, and K. K. Szabo, Phys. Lett. B **643**, 46 (2006).
[3] A. Bazavov *et al.*, Phys. Rev. D **85**, 054503 (2012).
[4] P. Costa, H. Hansen, M. C. Ruivo, and C. A. de Souza, Phys. Rev. D **81**, 016007 (2010).
[5] H. Mao, J. Jin, and M. Huang, J. Phys. G: Nucl. Part. Phys. **37**, 035001 (2010).
[6] E. S. Fraga, R. D. Pisarski, and J. Schaffner-Bielich, Phys. Rev. D **63**, 121702 (2001); Nucl. Phys. A **702**, 217 (2002).
[7] J. Schaffner-Bielich, J. Phys. G **31**, S651 (2005), and references therein.
[8] I. Sagert *et al.*, Phys. Rev. Lett. **102**, 081101 (2009).
[9] B. W. Mintz, E. S. Fraga, G. Pagliara, and J. Schaffner-Bielich, J. Phys. G **37**, 094066 (2010); Phys. Rev. D **81**, 123012 (2010).
[10] I. Bombaci, D. Logoteta, P. K. Panda, C. Providencia, and I. Vidana, Phys. Lett. B **680**, 448 (2009).
[11] Ph. Chomaz, M. Colonna, and J. Randrup, Phys. Rep. **389**, 263 (2004).
[12] J. Randrup, Phys. Rev. C **79**, 054911 (2009).
[13] H. Heiselberg, C. J. Pethick, and E. F. Staubo, Phys. Rev. Lett. **70**, 1355 (1993).
[14] K. Iida and K. Sato, Phys. Rev. C **58**, 2538 (1998).
[15] I. Bombaci, D. Logoteta, C. Providencia, and I. Vidana, A&A **528**, A71 (2011).
[16] D. N. Voskresensky, M. Yasuhira, and T. Tatsumi, Nucl. Phys. A **723**, 291 (2003).
[17] M. G. Alford, K. Rajagopal, S. Reddy, and F. Wilczek, Phys. Rev. D **64**, 074017 (2001).
[18] L. F. Palhares and E. S. Fraga, Phys. Rev. D **82**, 125018 (2010).
[19] A. Kurkela, P. Romatschke, A. Vuorinen, and B. Wu, arXiv:1006.4062 [astro-ph.HE].
[20] S. V. Molodtsov and G. M. Zinovjev, Phys. Rev. D **84**, 036011 (2011).
[21] O. Scavenius, Á. Mócsy, I. N. Mishustin, and D. H. Rischke, Phys. Rev. C **64**, 045202 (2001).
[22] J.-L. Kneur, M. B. Pinto, and R. O. Ramos, Phys. Rev. C **81**, 065205 (2010); L. Ferroni, V. Koch, and M. B. Pinto, *ibid.* **82**, 055205 (2010); AIP Conf. Proc. **1441**, 786 (2012).

[23] L. F. Palhares and E. S. Fraga, Phys. Rev. D **78**, 025013 (2008); E. S. Fraga, L. F. Palhares, and M. B. Pinto, *ibid.* **79**, 065026 (2009).
[24] R. W. Hasse and W. D. Myers, *Geometrical Relationships of Macroscopic Nuclear Physics* (Springer-Verlag, Berlin, 1988).
[25] Y. Nambu and G. Jona-Lasinio, Phys. Rev. **122**, 345 (1961); **124**, 246 (1961).
[26] C. Sasaki, B. Friman, and K. Redlich, Phys. Rev. D **77**, 034024 (2008).
[27] M. Buballa, Phys. Rep. **407**, 205 (2005).
[28] N. Itoh, Prog. Theor. Phys. **44**, 291 (1970); A. R. Bodmer, Phys. Rev. D **4**, 1601 (1971).
[29] E. Witten, Phys. Rev. D **30**, 272 (1984).
[30] P. Haensel, J. L. Zdunik, and R. Schaeffer, A&A **160**, 121 (1986).
[31] C. Alcock, E. Farhi, and A. Olinto, Astrophys. J. **310**, 261 (1986).
[32] P. Rehberg, S. P. Klevansky, and J. Hüfner, Phys. Rev. C **53**, 410 (1996).
[33] P. Costa, M. C. Ruivo, and C. A. de Sousa, Phys. Rev. D **77**, 096001 (2008).
[34] E. S. Bowman and J. I. Kapusta, Phys. Rev. C **79**, 015202 (2009).
[35] K. Fukushima, Phys. Rev. D **77**, 114028 (2008).
[36] J. E. Horvath, O. G. Benvenuto, and H. Vucetich, Phys. Rev. D **45**, 3865 (1992).
[37] M. L. Olesen and J. Madsen, Phys. Rev. D **49**, 2698 (1994); T. Fischer, S. C. Whitehouse, A. Mezzacappa, F. K. Thielemann, and M. Liebendorfer, Astron. Astrophys. **499**, 1 (2009).
[38] P. Costa, M. C. Ruivo, C. A. de Souza, and H. Hansen, Symmetry **2**, 1338 (2010).